Positional Isomers of Phenylacridine/Spirobifluorene as Deep-Blue Fluorescent Emitters for Organic Light-Emitting Diodes

Clement Brouillac, Fan-Cheng Kong, Joëlle Rault-Berthelot, Cassandre Quinton, Zuo-Quan Jiang, Cyril Poriel

Positional isomers of Phenylacridine/Spirobifluorene as Deep-Blue Fluorescent Emitters for Organic Light-Emitting Diodes

Clément Brouillac,[a] Fan-Cheng Kong,[b] Joëlle Rault-Berthelot,[a] Cassandre Quinton,[a] Zuo-Quan Jiang [b] and Cyril Poriel*[a]

a. Univ Rennes, CNRS, ISCR-UMR CNRS 6226, F-35000 Rennes, France.
email: cyril.poriel@univ-rennes1.fr
b. Institute of Functional Nano & Soft Materials (FUNSOM), Jiangsu Key Laboratory for Carbon-Based Functional Materials & Devices, Soochow University, Suzhou, Jiangsu 215123, China.

Keywords: Spirobifluorene, phenylacridine, deep-blue emitter, organic light-emitting diode, *spiro* compounds

Abstract

Designing deep-blue fluorophores with a low CIEy is an important request for organic light-emitting diode (OLED) technology either for display applications or to develop new applications such as light source with antibacterial properties. The challenge of deep-blue emitting OLEDs mainly relies on the difficulty to reach efficient emitters fulfilling all the characteristics desired to insure a high device performance with suitable CIE coordinates. In the present work, we report the synthesis, the physico-chemical properties and the application as emissive layer in an OLED of two deep-blue emitters constructed on the association of Spirofluorene-*N*-PhenylAcridine (**SPA-F**) and SpiroBiFluorene (**SBF**) molecular fragment. Two emitters, **2,2-SPAF-SBF** and **2,3-SPAF-SBF** have been constructed following a similar molecular design strategy, that is the connection of an electron rich SPA unit to a SBF backbone. The emission wavelength is tuned by the substitution pattern of the SBF backbone (*meta* or *para* linkage). Through a structure/properties relationship study, the electrochemical, photophysical and thermal/morphological properties of both emitters are discussed. When used as emitter in a multi-layer OLED, **2,2-SPA-SBF** displays a deep-blue emission reaching an EQE of ca 1.7% and a V_{on} of 4 V. The electroluminescent spectrum displays a λ_{max} below 400 nm (*i.e.* 394 nm) and CIE coordinates of (0.182, 0.054). The CIEy coordinate of 0.054 is low and fits the NTSC and EBU standards.

Introduction

In order to explore new organic light-emitting diodes (OLEDs) applications, an efficient emission on both ends of the visible spectrum *i.e.*, the violet[1-11] and near-infrared[12] regions is a central concern. For example, OLED emitting at short wavelengths can become an efficient antibacterial light source,[13] as many bacteria are sensible to a wavelength of 405 nm. More generally, in organic optoelectronics, high performance and stable deep blue OLEDs have always been the missing link of the technology, whatever the nature of emitters involved either fluorescent, phosphorescent or thermally activated delayed fluorescent.[14-18]

For the National Television Standards Committee (NTSC), the Commission Internationale de l'Eclairage (CIE) colour coordinates for a pure blue light are x=0.14 and y=0.08. For the European Broadcasting Union (EBU) (x=0.15/ y=0.06)[17, 19] and the International Telecommunication Union (ITU) (ITU-R Recommendation BT.2020: x=0.131/y=0.046), the y coordinate is decreased to very low values.[4] Researchers have tried, over the years, to reach these CIE coordinates, which are particularly difficult to obtain, especially the CIEy. Deep-blue fluorophores, efficient when used as emissive layer in an OLED with CIE coordinates in these ranges,[1-11] are difficult to design because many specific characteristics are mandatory. Intrinsically, a deep-blue emitter possesses a large energy gap (>3 eV), and it is therefore difficult to inject charges in such a material. The molecular design of such a fluorophore is therefore the key to reach a high efficiency OLED. Many design strategies have been studied over the years[16] and one of the most efficient consists to introduce an electron-rich (donor) and electron-poor (acceptor) moieties in the molecular structure. However, to keep the emission at a short wavelength, it is crucial to control the conjugation pathway and the intramolecular charge transfer (ICT) between the donor and acceptor functionalities, which can both cause a red shift

of the emission spectrum. In addition, the emission wavelength should also be maintained at a high energy at the solid state and therefore the supramolecular π–π interactions should be controled.[19] Add to that the fact that a high thermal/morphological stability is also a key property, and the difficulty to design an efficient deep-blue fluorophore is clearly highlighted. In the present work, two emitters, **2,2-SPAF-SBF** and **2,3-SPAF-SBF**, have been synthesized, studied and incorporated as emitter in an OLED. The molecules are extremely simple as based on the direct connection of two well-known molecular fragments in organic electronics, namely Spirofluorene-*N*-PhenylAcridine (SPAF) and SpiroBiFluorene (SBF).[4, 20-29] The emission is tuned by the substitution pattern of the SBF backbone either via a *para* linkage (C2 substitution) in **2,2-SPAF-SBF** or a *meta* linkage (C3 substitution) in **2,3-SPAF-SBF**. It is known that *para* and *meta* linkages provide different electron coupling between two molecular units and the π-conjugation extension is then affected. This strategy has appeared, in recent years, as an efficient tool to tune HOMO/LUMO energy levels, first singlet and triplet excited state and ICT, of great interest to design high efficiency materials for organic electronics.[22, 23] On the other hand, the PA core is known to be an efficient hole injecter due to its electron rich character.[23] Finally, in order to reach excellent physical properties, introduction of spiro carbon in the molecular structure is known to be an efficient strategy as initially shown by Salbeck and coworkers in the nineties.[21, 30, 31] The *spiro* connection also allows to control the interactions between two orthogonal functional units, a key feature to maintain an emission at short wavelength.[20, 21, 32-34] In the present work, the synthesis of these two blue emitters, their electrochemical, photophysical, and thermal properties and their application in OLED is presented. These emitters present, in the solid state, an emission in the deep-blue region, around 400 nm. When used as emitter in an OLED, a blue emission with CIE of (0.16, 0.05) and EQE of ca 1.7% is obtained for **2,2-SPAF-SBF**. The device presents a CIEy coordinate below 0.1, fitting the NSTC and EBU standards.

Synthesis

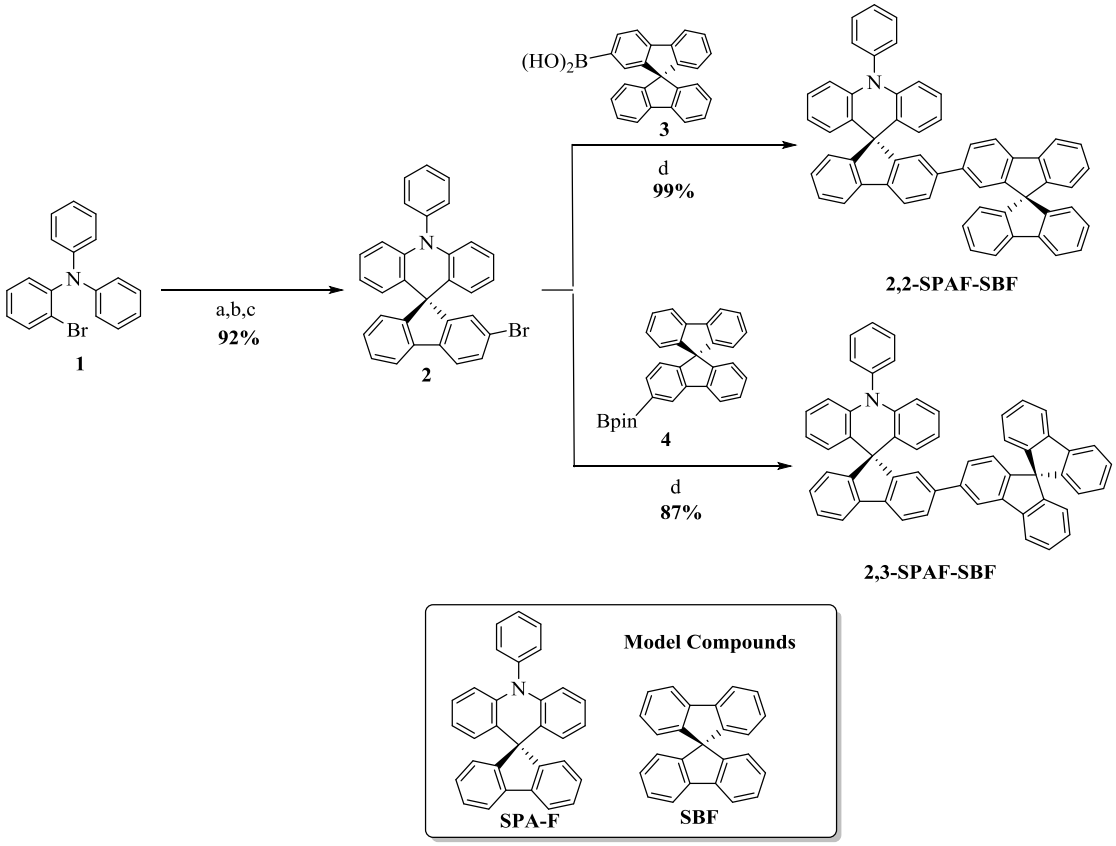

Figure 1. Synthesis of **2,2-SPAF-SBF** and **2,3-SPAF-SBF** (a. *n*-BuLi, THF, -78°C, 30 min; b. 2-bromofluorenone in THF, -78°C, 30 min; RT, 17 h, c. AcOH/HCl: 10/1 reflux 15 h, d. $Pd(dppf)_2Cl_2$, K_2CO_3, DMF reflux 17 h)

The future of electronic is undoubtedly based on organic semi-conductors, which can be efficiently synthesized, in other words with a high yield and a short number of steps. Both **2,2-SPAF-SBF** and **2,3-SPAF-SBF** have been synthesized at the gram scale, from commercially available starting materials using two well-known chemical reactions (Figure 1). The nucleophilic addition reaction of the lithiated intermediate derivatized from 2-bromotriphenylamine (**1**) on 2-bromofluorenone was the first step. Electrophilic intramolecular cyclization of the

resulting alcohol in a mixture of HCl and AcOH afforded the corresponding spirofluorenephenyalcridine (**2**) with the bromine atom attached at C2. Finally, a classical Suzuki coupling in the presence of either **3** or **4** provide the corresponding target molecules **2,2-SPAF-SBF** and **2,3-SPAF-SBF** with 91% and 79% of total yields respectively. In order to finely investigate the impact of the association presented herein, two model compounds will also be studied, namely spirobifluorene (**SBF)** and spirofluorenephenyalcridine (**SPA-F**), previously reported in literature.[22, 35]

Electrochemical Properties

The electrochemical properties have been investigated by cyclic voltammetry (CV) in CH_2Cl_2 for oxidation and in DMF for reduction, potentials are given versus a saturated calomel electrode (SCE).

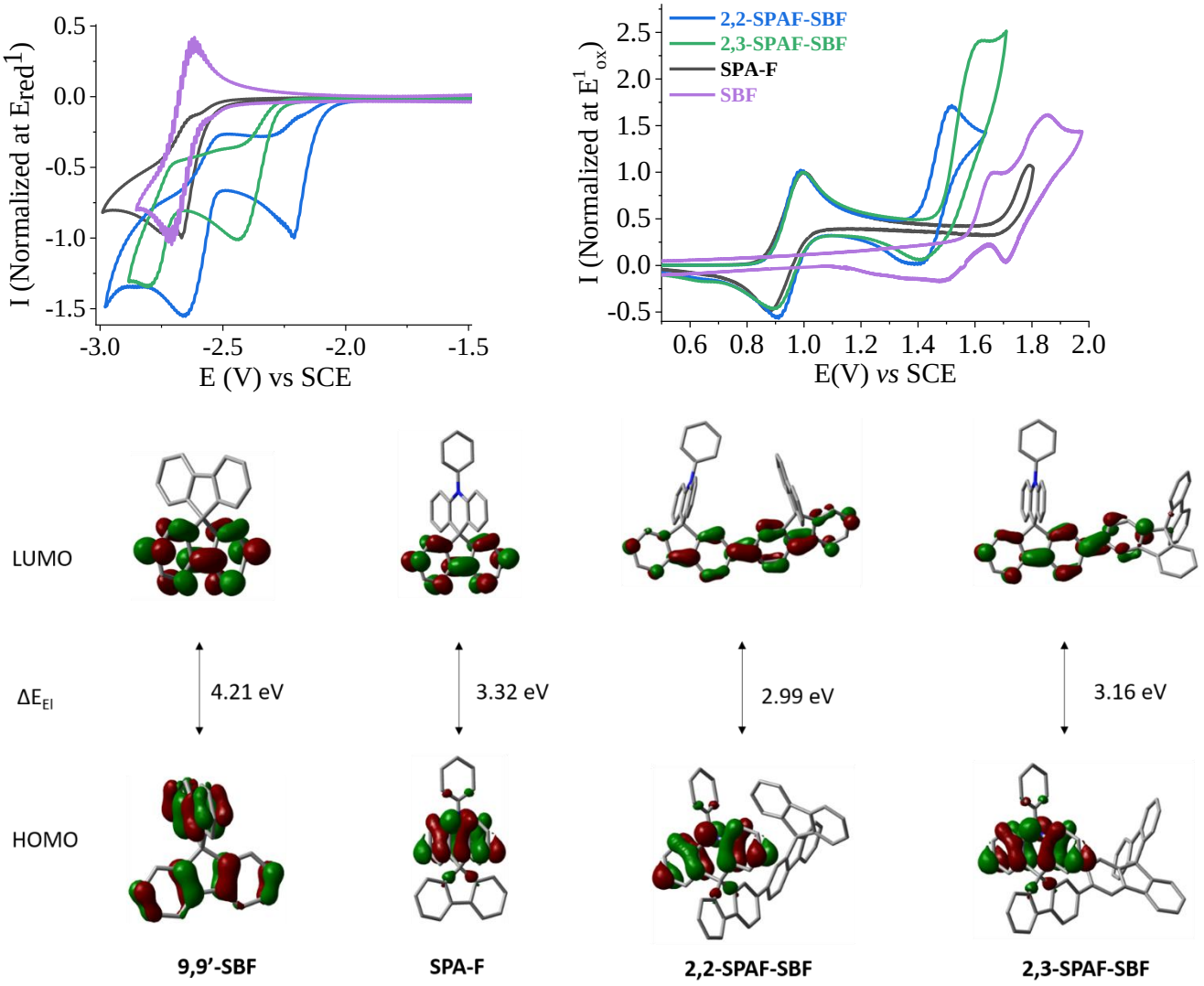

Figure 2. Normalized cyclic voltammograms of **2,2-SPAF-SBF** (blue lines), **2,3-SPAF-SBF** (green lines), **SPA-F** (black lines) and **SBF** (purple lines) in the cathodic (Top left, DMF + Bu_4NPF_6 0.1 M) or the anodic (Top right, CH_2Cl_2 + Bu_4NPF_6 0.2 M) range. Sweep-rate of 100 $mV.s^{-1}$, platinum disk (diameter 1 mm) working electrode. Representations of HOMO and LUMO orbitals obtained by DFT in B3LYP/6-311+G(d,p) (Bottom right).

Table 1. Selected electronic data

	2,2-SPAF-SBF	**2,3-SPAF-SBF**	**SPA-F**[23]	**SBF**[22]
λ_{abs}[nm][a] ($\varepsilon \times 10^4$ [L.mol^{-1}.cm^{-1}])	267, 308, 329	280, 298, 309, 320	269, 309	297, 308
$\lambda_{em\ sol}$ [nm][a, b]	363, 384, 403, 431	352, 368	348	310, 322
QY_{sol} [a, b, c]	0.52	0.06	-	0.55
$\lambda_{em\ film}$ [nm][b,d]	411, 437	411, 430	-	-
QY_{film} [d, e]	0.18	0.09	-	-
τ_s [ns][a,f]	2.2	3.7	1.5	4.6
k_r [ns^{-1}][g]	0.242	0.016	-	0.012
k_{nr} [ns^{-1}][g]	0.223	0.255	-	0.010
S_1 [eV][h]	3.62	3.76	-	4.13
HOMO (eV)[i]	-5.29	-5.28	-5.26	-5.95
LUMO (eV)[j]	-2.30	-2.12	-1.94	-1.74
ΔE_{El} (eV)[m]	2.99	3.16	3.32	4.21
HOMO th (eV)[l]	-5.26	-5.30	-5.29	-5.99
LUMO th (eV)[l]	-1.63	-1.48	-1.20	-1.26
T_d (°C)[m]	425	451	286	234[36]
T_g (°C)[n]	188	189	90	-
T_f (°C)[o]	357	-	141	199[36]
T_c (°C)[o]	230	-	281	135[36]

a. in cyclohexane at RT ; b. λ_{exc} =290 nm ; c. quantum yield (QY) determined with sulfate quinine in H_2SO_4 1 N as reference ; d. In spin-coated film; e. QY determined in integration sphere f. λ_{exc} =310 nm. g. k_r= QY/ τ_f and k_{nr}= $(1/\tau_f)\times(1-QY)$; h. from onset of emission spectrum in cyclohexane, $E(S_1)=1239.84/\lambda_{onset}$; i. in dichloromethane; j. in DMF; k. |HOMO-LUMO|; l. from DFT in B3LYP/6-311+G(d,p); m. from TGA; n. from 2nd cycle of heating of DSC; o. from 1st cycle of heating of DSC.

In oxidation, **2,2-SPAF-SBF**, **2,3-SPAF-SBF** and model compound **SPA-F** present a first reversible oxidation wave with a maximum at almost identical potential, ca 1 V (Figure 2, top right). This first electron transfer is therefore centred on the PA unit as confirmed by the localization of the HOMO, which is exclusively spread out on this fragment (Figure 2, bottom). As the first electron transfer of **SBF** is localized on one fluorene unit (Figure 2, bottom), this model compound presents a completely different cyclic voltammetry, with an oxidation shifted to higher potential (1.66 V). The HOMO energy levels of **2,2-SPAF-SBF**, **2,3-SPAF-SBF** were evaluated (from the onset of first wave) at -5.29 and -5.28 eV, almost identical to that of **SPA-F** (-5.26 eV)[23] but significantly higher to that of **SBF** (-5.95 eV).[22] The second oxidation is detected at higher potentials, 1.51 and 1.62 V for **2,2-SPAF-SBF** and **2,3-SPAF-SBF** respectively. This second electron transfer is assigned to the oxidation of the bifluorene fragment. Indeed, this wave is found at lower potential than the first observed in **SBF** (translating the different oxidation between a fluorene and a bifluorene) and is not present in **SPA-F**. In addition, there is a significant 110 mV difference between the two isomers, which translates the different π-conjugation pathways, induced by the different linkages. Indeed, the *para* linkage found in **2,2-SPAF-SBF** maximises the conjugation extension between the two linked fluorene units and then leads to a lower oxidation potential whereas the *meta* linkage found in **2,3-SPAF-SBF** decreases the electronic coupling between the two fluorene units and leads to a higher oxidation potential.

A different result was obtained in reduction as **2,2-SPAF-SBF** and **2,3-SPAF-SBF** display different CVs assigned to their different linkages. Both molecules display a first irreversible reduction wave with onset measured at -2.10 and -2.28 V respectively (Figure 2, left) giving a LUMO energy level of -2.30 and -2.12 eV. This difference in term of LUMO level is due to the different connection discussed above for the second oxidation wave. Indeed, in **2,2-SPAF-SBF**, the *para* linkage leads to a LUMO spread out on the four phenyl units of two linked fluorenes whereas in **2,3-SPAF-SBF**, it is only spread on three phenyl rings (Figure 2, bottom). This is also in accordance with the LUMO of both **SBF** and **SPA-F** measured at -1.74 eV[22] and -1.94 eV[23] respectively, which are significantly higher than those of **2,2-SPAF-SBF** and **2,3-SPAF-SBF** as only spread out on one fluorene. This difference in term of LUMO provides a gap contraction from 3.16 eV for **2,3-SPAF-SBF** to 2.99 eV for **2,2-SPAF-SBF**. These gaps are significantly contracted compared to the model compounds, highlighting the efficiency of the design strategy.

Photophysical Properties

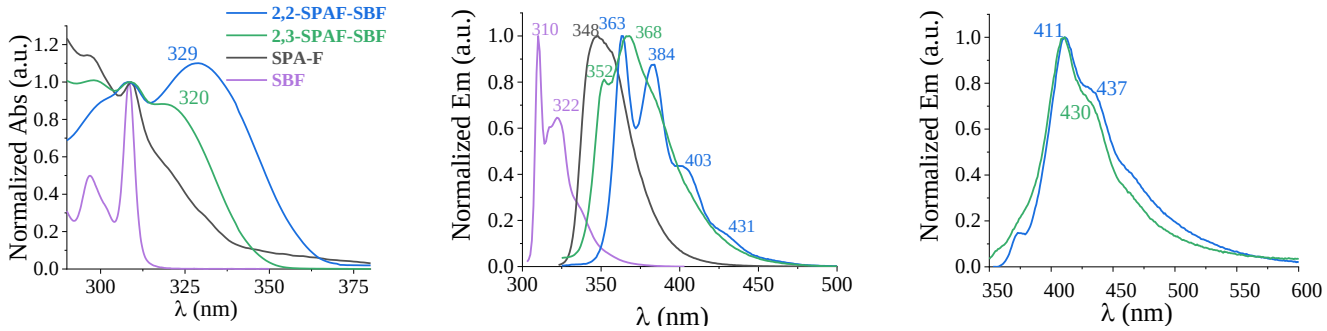

Figure 3. Absorption (Left) and emission in cyclohexane (Middle, λ_{exc} = 290 nm) and emission in spin-coated thin film (Right, λ_{exc} =290 nm) of **SBF**, **SPA-F**, **2,2-SPAF-SBF** and **2,3-SPAF-SBF**.

UV–Vis absorption and emission spectra of **2,2-SPAF-SBF** and **2,3-SPAF-SBF** were recorded in cyclohexane at room temperature (Figure 3). The optical properties are summarized in Table 1. We observe for **2,2-SPAF-SBF** a red shift of ca 9 nm of the band at low energy and an increase in absorption coefficient compared to that of **2,3-SPAF-SBF** (329 *vs* 320 nm). This feature is assigned to the difference of *para vs meta* linkages and the different π–conjugation pathway induced.[37] TD-DFT calculations (Figure 4) indicate that this band corresponds to a HOMO-1→LUMO transition with a high oscillator strength (f= 0.9337 and 0.7591 for **2,2-SPAF-SBF** and **2,3-SPAF-SBF** respectively), note that the *para* linkage provides a higher oscillator strength than *meta* linkage. It should be also precise that due to the spatial separation of HOMO and LUMO, the HOMO→LUMO transition has a very low oscillator strength close to 0. The band found at 309 nm is assigned to a transition involving molecular orbitals localized on the spirofluorene unit.

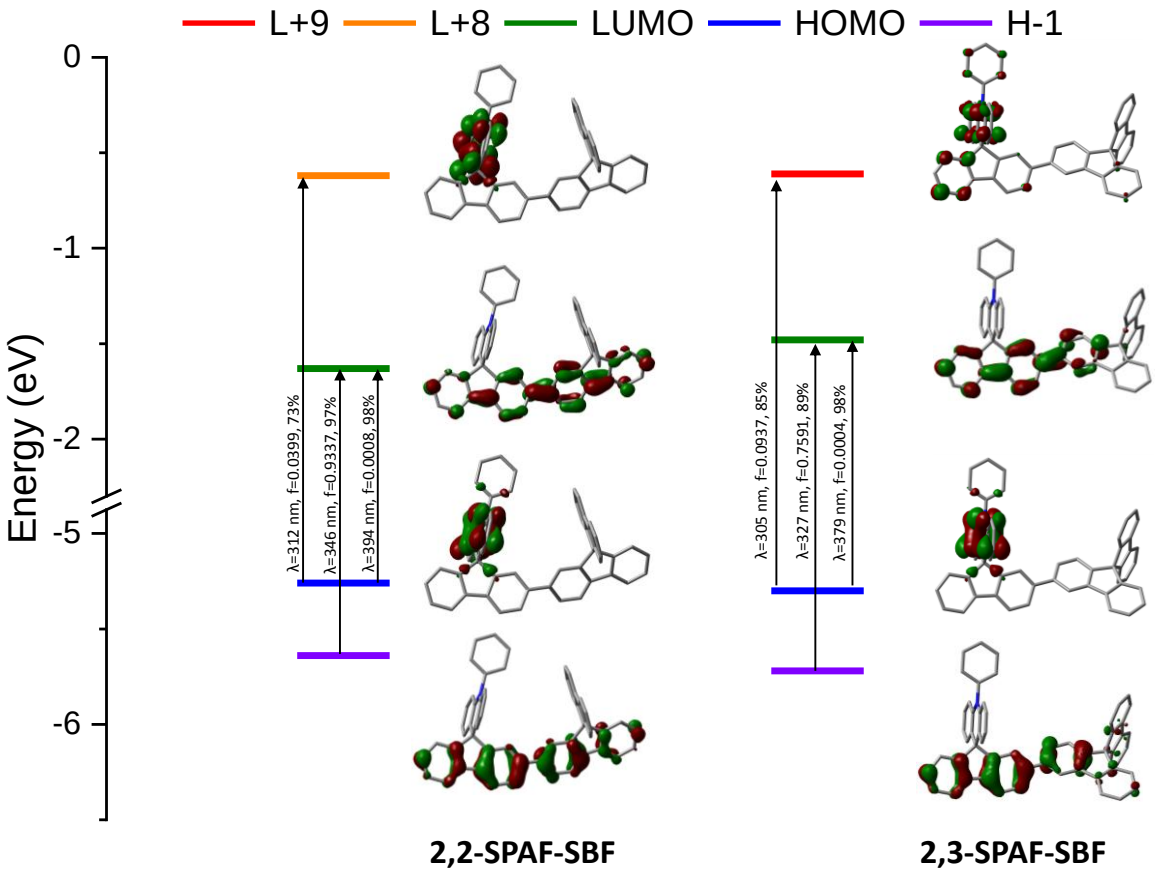

Figure 4. Representation of the energy levels and the main molecular orbitals involved in the electronic transitions of **2,2-SPAF-SBF** (left) and **2,3-SPAF-SBF** (right) obtained by TD-DFT b3lyp and the 6-311+G(d, p) basis set on the geometry of S_0, shown with an isovalues of 0.04 [e bohr-^{3}]$^{1/2}$ (for clarity purpose, only the main contribution for each transition is shown, details provided in SI).

In emission spectroscopy (cyclohexane), **2,2-SPAF-SBF** and **2,3-SPAF-SBF** present different spectra; the first one being well resolved and the last one not. For **2,2-SPAF-SBF**, the emission spectrum displays four bands at 363, 384, 403, and 431 nm, characteristic of fluorenes substituted at C2. [37, 38] In such a compound, it is known that the C-C bond linking the two fluorenes display a double bond character and therefore rigidified the system in accordance with the highly structured emission spectrum.[39, 40] **2,3-SPAF-SBF** displays a different spectrum, large and weakly resolved. The difference in term of wavelengths (352 *vs* 363 nm) is similar to that observed in absorption, ca 11 nm and is due to linkages effects described above. Both fluorophores display an emission in the deep-blue region. Compare to model compounds, **SPA-F** and **SBF**, which possess an emission wavelength at 348[23] and 310[22] nm respectively, one can note, the clear extension of the conjugation pathway, induced by the direct connection of PA and SBF units. The main difference observed between the two emitters is linked to their quantum yields. Indeed, the quantum yields of **2,2-SPAF-SBF** and **2,3-SPAF-SBF** are measured at 0.52 and 0.06 respectively. The analysis of the radiative (k_r) and the non-radiative (k_{nr}) constants gives the origin of this quantum yield difference. For both molecules, the k_{nr} are almost identical (0.22 / 0.26 ns^{-1} for **2,2-SPAF-SBF** / **2,3-SPAF-SBF** respectively) in accordance with the similitude of the molecular structures, which in turn provides similar vibrational deactivation pathways. However, the k_r are very different (0.242 / 0.016 ns^{-1} for **2,2-SPAF-SBF/ 2,3-SPAF-SBF** respectively) in accordance with the oscillator strengths difference observed between the S_0 and S_1 states (see above). This is the direct consequence of the *para* and *meta* linkages.

Solid state fluorescence has finally been recorded before incorporation in OLED devices. From solution to film, there is a red shift detected for the two emitters and both molecules display an almost superimposable spectrum with λ_{max} measured at 411 nm. Thus, the emission is maintained in the deep-blue region, which is highly beneficial for the targeted application (see below). Herein, the quantum yield in the solid state, is particularly important as it can drastically drop compare to the solution. In the present design, the two spiroconnected fluorenes allow to avoid strong intermolecular interactions and the quantum yield is maintain at 0.18 and 0.09 for **2,2-SPAF-SBF** and **2,3-SPAF-SBF**.

Thermal Properties

Before any possible OLED application, thermal properties should be evaluated by means of thermogravimetric analyses (TGA) and differential scanning calorimetry (DSC), Figure 5. In the present case, the two emitters possess a high decomposition temperature T_d (5% mass loss), above 400°C (425 and 451 nm for **2,2-SPAF-SBF** and **2,3-SPAF-SBF** respectively). More importantly, **2,2-SPAF-SBF** and **2,3-SPAF-SBF** present the same high glass transition temperature T_g (188-189°C determined by DSC during the 2nd heating run, between 0 and 275°C). Both high T_g and high T_d parameters are important to reach highly stable devices. It is important to notify that no crystallization temperature is observed for the both compounds, which is highly beneficial for OLED applications.

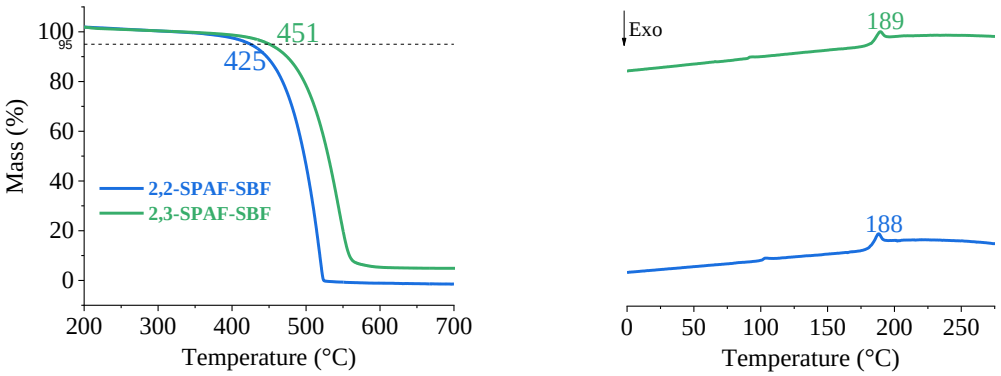

Figure 5. TGA (Left) and DSC (Right, 2nd heating cycle only) of **2,2-SPAF-SBF** (blue lines) and **2,3-SPAF-SBF** (green lines).

Electroluminescent Properties

Finally, **2,2-SPAF-SBF** and **2,3-SPAF-SBF** were used as emitter in a multi-layer OLED stack. The device configuration was ITO/HAT-CN (10 nm)/ TAPC (40 nm)/ TCTA (10 nm)/ mCP: emitters (2%, 20 nm)/ TmPyPB (40 nm)/ Liq (2 nm)/ Al (120 nm). The concentration of the emitter in the emissive layer was varied between 2 and 10% and the most efficient reported at 2%.

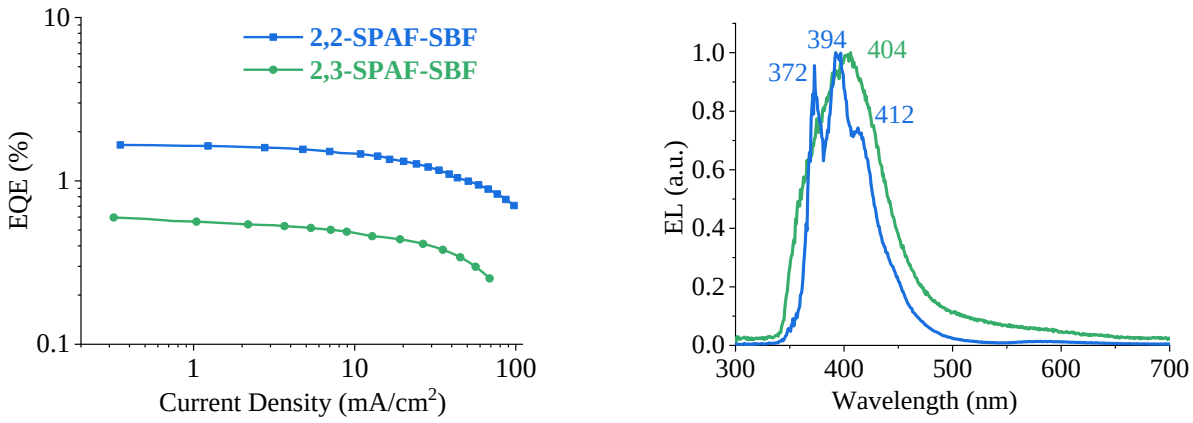

Figure 6. EQE vs current density (A) and electroluminescent spectra (B) of **2,2-SPAF-SBF** and **2,3-SPAF-SBF**

The electroluminescent (EL) spectra of **2,3-SPAF-SBF**, measured at a current density of 10 mA/cm^2, displays a maximum at 404 nm (Figure 6B), very similar to the one obtained in solid state fluorescence. Its positional isomer **2,2-SPAF-SBF** presents a more resolved spectrum with a maximum detected at a lower wavelength of 394 nm. For **2,3-SPAF-SBF**, the full width at half-maximum (FWHM) is significantly increased from solid state emission (52 nm) to electroluminescence (81 nm) whereas for **2,2-SPAF-SBF**, this difference remains weak (55 vs 61 nm). This allows to keep a low CIEy coordinate in the case of **2,2-SPAF-SBF** (0.054) whereas that of **2,3-SPAF-SBF** is almost double, *i.e.* 0.098 (Table 2). Thus, the CIE coordinates of the **2,2-SPAF-SBF** based OLED (0.181, 0.054) appears to be very interesting for display, with a particularly low CIEy value of 0.054. The current density versus EQE plots for these devices are presented Figure 6and the OLED efficiencies are gathered Table 2. The turn-on voltages (V_{on} at 1 Cd.m^{-2}) of these devices are measured between 3.7 and 4.0 V, in the same range than those obtained with the best fluorescent violet OLEDs reported to date in literature (3.6-3.8 V).[4, 11] This can be assigned to the presence of the PA unit and indicates the efficiency of such a design. The EQE of **2,3-SPAF-SBF** was measured at a low value of 0.6%, whereas that of **2,2-SPAF-SBF** was increased by almost a factor 3 and an EQE of 1.66 %, with a very low concentration of emitter (2%). This difference in term of device performance can be related to that observed in term of quantum yield (Table 1). Thus, despite the emission wavelengths of **2,2-SPAF-SBF** and **2,3-SPAF-SBF** are close, the emission efficiency is clearly in favour of the former. This is again an important characteristic of the *para* linkage, which allows maintaining a higher quantum yield compare to its *meta* counterpart, as previously reported in literature for structurally related molecular systems.[22, 37] The performance of **2,2-SPAF-SBF** based OLEDs with a V_{on} of 4V, an EQE of ca 1.66% and CIE coordinate of (0.182, 0.054) is a first step towards the development of high efficiency violet devices with low CIEy and approach the EBU and ITU recommendations.

Table 2. Best OLED performances using **2,2-SPAF-SBF and 2,3-SPAF-SBF** as emitter (Device structure:ITO/HAT-CN (10 nm)/ TAPC (40 nm)/ TCTA (10 nm)/ mCP: emitters (2%, 20 nm)/ TmPyPB (40 nm)/ Liq (2 nm)/ Al (120 nm).

Dopant	V_{on} [a] (V)	CE_{max} [b] (cd/A)	PE_{max} [b] (lm/W)	EQE_{max} [b] (%)	λ_{max} [c] (nm)	CIE [c] (x, y)
2,2-SPAF-SBF	4.0	0.25	0.20	1.66	394	(0.181, 0.054)
2,3-SPAF-SBF	3.7	0.19	0.15	0.60	404	(0.182, 0.098)

a. Recorded at a luminance of 1 cd/m^2. b. The maximum CE, PE and EQE. c. Measured at a driving current density of 10 mA/cm^2.

Conclusion

To conclude, we report in this work the synthesis, the physico-chemical properties and the application in OLED of two deep blue emitters constructed on the association of a phenylacridine-fluorene unit and a spirobifluorene core. These materials, which are positional isomers, can be easily synthesized and present (i) solid state emission wavelength around 400 nm, (ii) excellent thermal/morphological properties, and (iii) a low first oxidation potential (1 V vs SCE). The positional isomerism drives nevertheless the quantum yield in the solid state, which appearS to be low for **2,3-SPAF-SBF** and high for **2,2-SPAF-SBF**. When incorporated as emitter, at a very low concentration of 2%, in the emissive layer of an OLED, **2,2-SPAF-SBF** displays a deep-blue emission with CIE of (0.181, 0.054), a maximum EQE of 1.66% and a V_{on} of 4 V. This CIEy coordinate fits the NTSC and EBU standards. To further improve the OLED performance, phenylacridine-like fragments such as quinolinophenothiazine[41, 42] or quinolinoacridine,[43-46] widely used nowadays in organic electronics, could offer an interesting alternative.

There are no conflicts to declare.

Supporting Information

Details on the materials synthesis, their thermal, photophysical and electrochemical properties, theoretical modeling and device data are provided in the supporting Information. Copies of NMR spectra are also included. The Supporting Information is available free of charge on the Publications website.

Acknowledgments

The authors would like to thank the ANR (SPIROQUEST, n°19-CE05-0024 and ANR-22-CE07-0041) for financial support of this project, the Agence de l'Environnement et de la Maitrise de l'Energie (ADEME) for PhD grand (CB, EcoElec Project). We would like to thank GENCI (N°AD0100805032R1) and the Inorganic Theoretical Chemistry (CTI) Team at ISCR for generous allocation of computational time, Bruno Lafitte (ADEME), and the CRMPO (Rennes) for mass analysis. The authors thank Dr J. F. Bergamini (Rennes) for the TOC material.

Received: ((will be filled in by the editorial staff))

References

[1]Y. Zhang, G. Cheng, Y. Zhao, J. Hou, S. Liu, S. Tang, Y. Ma, *App. Phys. Lett.* **2005**, *87*, 241112.
[2]H. L. Lee, W. J. Chung, J. Y. Lee, *Small* **2020**, *16*, 1907569.
[3]H. Liu, L. Kang, J. Li, F. Liu, X. He, S. Ren, X. Tang, C. Lv, P. Lu, *J. Mater. Chem. C* **2019**, *7*, 10273-10280.
[4]S. N. Zou, X. Chen, S. Y. Yang, S. Kumar, Y. K. Qu, Y. J. Yu, M. K. Fung, Z. Q. Jiang, L. S. Liao, *Adv. Opt. Mater.* **2020**, *8*, 2001074.
[5]J. Zhao, B. Liu, Z. Wang, Q. Tong, X. Du, C. Zheng, H. Lin, S. Tao, X. Zhang, *ACS Appl. Mater. Interfaces* **2018**, *10*, 9629-9637.
[6]W.-C. Chen, Y. Yuan, S.-F. Ni, Q.-X. Tong, F.-L. Wong, C.-S. Lee, *Chem. Sci.* **2017**, *8*, 3599-3608.
[7]B. Liu, Z.-W. Yu, D. He, Z.-L. Zhu, J. Zheng, Y.-D. Yu, W.-F. Xie, Q.-X. Tong, C.-S. Lee, *J. Mater. Chem. C* **2017**, *5*, 5402-5410.
[8]X. Wang, Y. Wu, C. M. Wu, Y. Li, D. Wang, Y. Wu, S. Ning, B. Jiao, Z. Wu, *New. J. Chem.* **2022**, *46*, 419-425.
[9]Z. Li, C. Li, Y. Xu, N. Xie, X. Jiao, Y. Wang, *J. Phys. Chem. Lett.* **2019**, *10*, 842-847.
[10]C. Brouillac, W.-S. Shen, J. Rault-Berthelot, O. Jeannin, C. Quinton, Z.-Q. Jiang, C. Poriel, *Mater. Chem. Front.* **2022**, *6*, 1803-1813.
[11]G. Li, M. Xia, J. Liu, J. Zheng, B. Zhao, H. Peng, *Dyes Pigm.* **2023**, *213*, 111183.
[12]Y. Yuan, Y. Hu, Y.-X. Zhang, J.-D. Lin, Y.-K. Wang, Z.-Q. Jiang, L.-S. Liao, S.-T. Lee, *Adv. Funct. Mater.* **2017**, *27*, 1700986.
[13]M. Maclean, L. E. Murdoch, S. J. MacGregor, J. G. Anderson, *Photochem. Photobiol.* **2013**, *89*, 120-126.
[14]J.-H. Lee, C.-H. Chen, P.-H. Lee, H.-Y. Lin, M.-k. Leung, T.-L. Chiu, C.-F. Lin, *J. Mater. Chem. C* **2019**, *7*, 5874-5888.
[15]Y. Wang, J. H. Yun, L. Wang, J. Y. Lee, *Adv. Funct. Mater.* **2020**, *31*, 2008332.
[16]C. Poriel, J. Rault-Berthelot, *Adv. Funct. Mat.* **2020**, *30*, 1910040.
[17]X. Yang, X. Xu, G. Zhou, *J. Mater. Chem. C* **2015**, *3*, 913-944.
[18]A. Monkman, *ACS Appl. Mater. Interfaces* **2022**, *14*, , 20463–20467.
[19]F. Dumur, in *Advanced Surface Engineering Materials*, Scrivener Publishing, **2016,** 561-634.
[20]Y.-K. Qu, Q. Zheng, J. Fan, L.-S. Liao, Z.-Q. Jiang, *Acc. Mater. Res.* **2021**, *2*, 1261-1271.
[21]T. P. I. Saragi, T. Spehr, A. Siebert, T. Fuhrmann-Lieker, J. Salbeck, *Chem. Rev.* **2007**, *107*, 1011-1065.
[22]C. Poriel, C. Quinton, F. Lucas, J. Rault- Berthelot, Z. Q. Jiang, O. Jeannin, *Adv. Funct. Mater.* **2021**, 2104980.
[23]F. Lucas, C. Quinton, S. Fall, T. Heiser, D. Tondelier, B. Geffroy, N. Leclerc, J. Rault-Berthelot, C. Poriel, *J. Mater. Chem. C* **2020**, *8*, 16354-16367.
[24]P. Tourneur, F. Lucas, C. Quinton, Y. Olivier, R. Lazzaroni, P. Viville, J. Cornil, C. Poriel, *J. Mater. Chem. C* **2020**, *8*, 14462-14468.
[25]P. Tourneur, F. Lucas, C. Brouillac, C. Quinton, R. Lazzaroni, Y. Olivier, P. Viville, C. Poriel, J. Cornil, *Adv. Photonics Res.* **2022**, 2200124.
[26]C. Poriel, J. Rault-Berthelot, *Acc. Mater. Res.* **2022**, *3*, 379-390.
[27]X.-D. Zhu, C.-C. Peng, F.-C. Kong, S.-Y. Yang, H.-C. Li, S. Kumar, T.-T. Wang, Z.-Q. Jiang, L.-S. Liao, *J. Mater. Chem. C* **2020**, *8*, 8579-8584.
[28]X.-Y. Liu, Y.-J. Zhang, X. Fei, M.-K. Fung, J. Fan, *Chem. Eur. J.* **2019**, *25*, 6788-6796.

[29]X.-D. Zhu, Y.-L. Zhang, Y. Yuan, Q. Zheng, Y.-J. Yu, Y. Li, Z.-Q. Jiang, L.-S. Liao, *J. Mater. Chem. C* **2019**, *7*, 6714-6720.
[30]J. Salbeck, N. Yu, J. Bauer, F. Weissörtel, H. Bestgen, *Synth. Met.* **1997**, *91*, 209-215.
[31]R. Pudzich, T. Fuhrmann-Lieker, J. Salbeck, *Adv. Polym. Sci.* **2006**, *199*, 83-142.
[32]L.-H. Xie, J. Liang, J. Song, C.-R. Yin, W. Huang, *Curr. Org. Chem.* **2010**, *14*, 2169-2195.
[33]S. Liu, D. Xia, M. Baumgarten, *ChemPlusChem* **2021**, *21*, 36-48.
[34]C. Poriel, L. Sicard, J. Rault-Berthelot, *Chem. Comm.* **2019**, *55*, 14238-14254.
[35]F. Lucas, O. A. Ibraikulov, C. Quinton, L. Sicard, T. Heiser, D. Tondelier, B. Geffroy, N. Leclerc, J. Rault-Berthelot, C. Poriel, *Adv. Opt. Mater.* **2020**, *8*, 1901225.
[36]S. Thiery, D. Tondelier, C. Declairieux, G. Seo, B. Geffroy, O. Jeannin, J. Rault-Berthelot, R. Métivier, C. Poriel, *J. Mater. Chem. C* **2014**, *2*, 4156-4166.
[37]L. Sicard, C. Quinton, J.-D. Peltier, D. Tondelier, B. Geffroy, U. Biapo, R. Métivier, O. Jeannin, J. Rault-Berthelot, C. Poriel, *Chem. Eur. J.* **2017**, *23*, 7719-7723.
[38]J. Robin, N. Audebrand, C. Poriel, J. Canivet, G. Calvez, T. Roisnel, V. Dorcet, P. Roussel, *CrystEngComm* **2017**, *19*, 2042-2056.
[39]J.-F. Wang, J.-K. Feng, A.-M. Ren, L. Yang, *Chin. J. Chem.* **2005**, *23*, 1618-1624.
[40]G. Heimel, M. Daghofer, J. Gierschner, E. J. W. List, A. C. Grimsdale, K. Müllen, D. Beljonne, J. L. Brédas, E. Zojer, *J. Chem. Phys.* **2005**, *122*, 054501-054511.
[41]F. Lucas, D. Tondelier, B. Geffroy, T. Heiser, O. A. Ibraikulov, C. Quinton, C. Brouillac, N. Leclerc, J. Rault-Berthelot, C. Poriel, *Mater. Chem. Front.* **2021**, *5*, 8066-8077.
[42]F. Lucas, C. Brouillac, S. Fall, N. Zimmerman, D. Tondelier, B. Geffroy, N. Leclerc, T. Heiser, C. Lebreton, E. Jacques, C. Quinton, J. Rault-Berthelot, C. Poriel, *Chem. Mater.* **2022**, *34*, 8345–8355.
[43]A. Khan, Y.-K. Wang, C.-C. Huang, S. Kumar, M.-K. Fung, Z.-Q. Jiang, L.-S. Liao, *Org. Electron.* **2020**, *77*, 105520.
[44]Y.-K. Wang, S.-H. Li, S.-F. Wu, C.-C. Huang, S. Kumar, Z.-Q. Jiang, M.-K. Fung, L.-S. Liao, *Adv. Funct. Mater.* **2018**, *28*, 1706228.
[45]Y.-K. Wang, S.-F. Wu, Y. Yuan, S.-H. Li, M.-K. Fung, L.-S. Liao, Z.-Q. Jiang, *Org. Lett.* **2017**, *19*, 3155-3158.
[46]S. Y. Yang, Z. Q. Feng, Z. Fu, K. Zhang, S. Chen, Y. J. Yu, B. Zou, K. Wang, L. S. Liao, Z. Q. Jiang, *Angew Chem Int Ed Engl* **2022**, e202206861.